Available online at www.sciencedirect.com
ScienceDirect
Polymer 48 (2007) 3273–3285
polymer
www.elsevier.com/locate/polymer

Shear induced crystallization of poly(*m*-xylylene adipamide) with and without nucleating additives

Sophie Naudy [a,b,c], Laurent David [a,b,c], Cyrille Rochas [d], René Fulchiron [a,b,c,*]

[a] *Université de Lyon, Lyon F-69003, France*
[b] *Université de Lyon 1, IMP/LMPB Laboratoire des Matériaux Polymères et Biomatériaux, Villeurbanne F-69622, France*
[c] *CNRS, UMR5223, Ingénierie des Matériaux Polymères, Villeurbanne F-69621, France*
[d] *Laboratoire de Spectrométrie Physique UJF UMR CNRS #5588, Université Joseph Fourier, 38402 Saint Martin d'Hères Cedex, France*

Received 14 November 2006; received in revised form 7 March 2007; accepted 24 March 2007
Available online 6 April 2007

Abstract

The shear induced crystallization of the poly(*m*-xylylene adipamide) (MXD6) which is a semi-aromatic polyamide, was studied for a virgin (PA1) and a nucleated (PA2) grades using a shearing hot stage coupled with a microscope. Half crystallization times were measured according to the crystallization conditions (crystallization temperature, shear rate and shearing time). The effect of shear on the crystallization kinetics was shown by a strong decrease of the crystallization times for both materials. PA2 sensitivity to shear was much lower than that of PA1. This was attributed to the presence of nucleating agents which increased the primary nucleation density in the unsheared quiescent melt, leading to a higher necessary shear rate to overcome the quiescent nucleation. Kinetic models were proposed to predict the crystallization process as a function of the crystallization conditions. They were based on both Avrami and Hoffman–Lauritzen theories and modified to take into account the effect of shear. In the model the nucleation rate of the crystalline entities was related to the shear rate by a power function. Besides, crystalline morphology and orientation were studied by wide and small angle X-ray scattering to confirm the orientation effect of the shear in the crystalline part of the material.

Keywords: Poly(*m*-xylylene adipamide); Shear induced crystallization; X-ray analysis

1. Introduction

The final properties of semi-crystalline thermoplastic polymer materials are directly related to the crystalline morphology formed during processing. Therefore, the study of the crystalline morphology development is of major interest for industrial as well as for fundamental research for the understanding and the prediction of the crystallization mechanisms in different conditions and for various polymer formulations.

The processing of polymers generates high strain in these materials so that the macromolecular chains' orientation affects the development of the crystalline morphology. It is well known that applying a shear before and/or during the crystallization process will enhance the kinetics and change the resulting morphology [1–10].

In order to measure this kinetics enhancement, numerous homemade devices were previously used. Two kinds of measurement are preferentially developed: rheo-optic devices, like shearing hot stage coupled with optical microscope [1–7] or rheometry apparatus [5,8,9]. From a methodological point of view, some studies expected to simulate the complex flow occurring during processing [4,10] whereas other studies tried to well control the thermal and shear conditions [1,2,5,6,8].

* Corresponding author. Université de Lyon 1, IMP/LMPB Laboratoire des Matériaux Polymères et Biomatériaux, Bat ISTIL, 43 bd du 11 novembre, Villeurbanne F-69622, France.
E-mail address: rene.fulchiron@univ-lyon1.fr (R. Fulchiron).

0032-3861/$ - see front matter © 2007 Elsevier Ltd. All rights reserved.
doi:10.1016/j.polymer.2007.03.076

Even if the experimental devices were different, the general trend in such studies is that the acceleration of the crystallization is due to the orientation of the macromolecular chains which promotes the nucleation [1,5,7,8]. This effect of shear largely depends on the shear intensity and the crystallization temperature. The existence of a critical shear rate above which the shear flow efficiently speeds up the crystallization process is often described [1,2]. Practically, the shear effect is revealed by a decrease of the crystallization characteristic time which can be either the induction time [1,2] or the half crystallization time (half conversion time) [4,5,11]. The modification of the semi-crystalline morphology which turns from spherulitic entities to oriented structures after very high shear treatments is also well known [3,4,11]. The increase of the nucleation density is largely described [3,4,6,8] but only a few studies managed to quantify it [1,5,7,11]. The influence of the shear on the lamellar growth rate G_R is more debated but most of the works seem to show that it is not affected by the shear if the shear duration remains short compared to the crystallization time [5,7,11].

The prediction of the crystallization kinetics in quiescent conditions is based on the classical theories of Avrami [12–14], Ozawa [15] or Nakamura [16,17]. One of the disadvantages of these models is that they do not take into account the process of secondary crystallization which can be important for polyamides for example. Moreover, the shear effect in Avrami based equations was phenomenologically introduced by modifying the exponent n for which values has been reported up to 7 [18] and even up to 12 [1] although usual theory predicts integer values between 1 and 3. Alternatively, Masubuchi et al. [9] introduced an induction time for the modeling of the crystallization kinetics. Other models were established by taking into account the increase of the number of activated nuclei due to shear flow. This was related to the shear intensity with a combination of two parameters, namely the shear rate $\dot{\gamma}$ and the shearing time t_s [10] or to their product $\dot{\gamma}t_s$ [7]. More recently, the nucleation was related to the flow relaxation time of the chains, considering that this parameter governs the ability of the molecules to be aligned by the strain [5,19–24].

The semi-aromatic poly(*m*-xylylene adipamide) (MXD6) was first synthesized in the early 1950s by Carlston and Lum from *m*-xylylenediamine and adipic acid [25,26]. Fig. 1 shows its chemical structure. Its crystalline unit cell was investigated by X-ray diffraction and infrared spectroscopy during the 1960s by Ota et al. [27]. The unit cell is triclinic with the following parameters: $a = 1.201$ nm; $b = 0.483$ nm; $c = 2.98$ nm; $\alpha = 75.0°$; $\beta = 26.0°$; $\gamma = 65.0°$. Only a few works deal with the crystallization of MXD6. Single crystals of MXD6 were elaborated by slow cooling of a dilute glycerine solution [28] and crystallization induced by water sorption was investigated by Inoue [29].

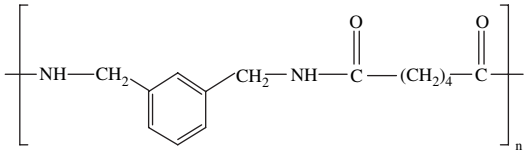

Fig. 1. Chemical structure of MXD6.

Measurements of the MXD6 crystallization kinetics in quiescent conditions were investigated and predicted by kinetic models based on the Avrami and Ozawa theories according to the crystallization conditions. All the results are detailed in our previous paper [30]. Fundamental constants such as the thermodynamic melting point T_m^0 or both constants to describe the lamellae growth rate K_g and G_0 (see Eq. (2) below) were determined from isothermal crystallization experiments.

The present study proposes the measurement of the shear induced crystallization kinetics mainly by a rheo-optic technique. Some of the results dealing with the quiescent crystallization of the virgin and nucleated MXD6 will be recalled as they are considered as the reference behavior. The effect of shear will be described as a function of the shear rate, shearing time and temperature. A kinetic model is developed to depict the experimental values. It is based on the Avrami theory coupled with the Hoffman–Lauritzen prediction of the growth rate [31] and modified to take into account the increase of activated nuclei due to the shearing treatment.

2. Materials and methods

2.1. Materials

Two grades based on MXD6 were studied. The first one consisted in a virgin MXD6 labeled PA1 supplied by Solvay. The weight average molecular weight and the polydispersity index of this initial MXD6 measured by SEC were 33,200 g/mol and 2.65, respectively. The second one, labeled PA2 was a nucleated formulation consisting in a blend of this MXD6 with 11% of PA 66 and 1% of talc (Steamic 00S from talc de Luzenac) whose particle size characteristics are: mean cut diameter $d_{50\%} = 1.8$ μm and top cut diameter $d_{98\%} = 6.2$ μm and the specific surface area is 11 m^2/g. The blend was achieved using a laboratory twin-screw extruder without no specific dispersion difficulty.

2.2. Rheo-optic measurements

Quiescent and shear induced crystallization experiments were carried out in the shearing hot stage CSS 450 from Linkam Scientific Instruments UK coupled with an optical microscope Orthoplan from Leitz. Pellets (about 20 mg) were placed in the shearing device when the two plates were hot. The gap was set to 75 μm after the sample melting. The sample was molten at 280 °C for 4 min to erase its thermal history and then cooled at 30 °C/min (which is the maximum available). As soon as the crystallization temperature was reached, the shearing step defined by a shear rate and a shearing time was applied and data collection (pictures or transmitted light intensity) started. The steady shearing step before crystallization was called preshear. Each measurement was performed two or three times to obtain an average value of the half crystallization time.

Crystallization kinetics were obtained from the variation of the transmitted light intensity $I(t,T)$. Even if the quantitative relation between the crystallization advancement and the transmitted light is not direct, the relative crystallinity α was estimated by the relative decrease of the transmitted light intensity:

$$\alpha(t,T) = \frac{I_0 - I(t,T)}{I_0 - I_\infty} \quad (1)$$

where I_0 is the initial light intensity and I_∞ is the final value.

It must be mentioned that this experimental procedure for estimating the relative crystallinity was already used and validated by comparing the obtained crystallization times without shear and those obtained with differential scanning calorimetry (DSC) [5,30]. Moreover, the correlation between the entire DSC and light intensity signals was also shown for polylactide crystallization [32].

2.3. X-ray measurements

Small angle X-ray scattering (SAXS) as well as wide angle X-ray diffraction (WAXD) were performed at the ESRF (Grenoble France) on the BM2 beamline. The data were collected at an incident photon energy of 16 keV. A bi-dimensional detector (CCD camera from Ropper Scientific) was used. All the data were corrected thanks to the software Bm2Img available on the beamline that meant dark current (*i.e.* non-illuminated camera), flat field response (*i.e.* homogeneously illuminated camera) and tapper distortion. Moreover, the contribution of the empty cell was subtracted to the scattering curves of the studied samples. The calculation of the scattering vector values q or the scattering angles 2θ was performed thanks to the use of the standard silver behenate [33].

The generation of the sheared samples devoted to X-ray measurements was obtained using a parallel plate cell of a Rheometrics RMS 800 rheometer (diameter 8 mm, gap 500 μm). A few pellets were placed in the rheometer cell and were molten in the same melting conditions than for rheo-optic measurements. Then it was cooled down to the required crystallization temperature. As soon as this temperature was reached, the desired shear treatment was carried out. The sample was then kept at this temperature until the crystallization was achieved. This was checked thanks to the simultaneous measurement of the dynamic modulus at a frequency of 1 rad/s with a strain of approximately 1%. The solidification was considered complete when the modulus became constant after its increase due to the crystallization. Obviously, due to the parallel plate geometry, the shear rate in the sample was not constant. Therefore the X-ray measurements were carried out on a piece of 2 mm diameter which was extracted from the peripheral area of the sample, where the shear rate is the greatest and corresponds to the command value of the rheometer. In this small extracted sample, the shear rate was considered to be constant.

Small samples were positioned horizontally or vertically (perpendicular to the beam) on a rotating and translating sample holder (designed by the LIM–ENSAM Paris) so that the sample could be oriented with a controlled angle. The distance between the sample center and the camera was about 6.2 cm for WAXD measurements and about 164 cm for SAXS measurements.

3. Results and discussion

3.1. Static crystallization [30]

The crystallization behaviors of both PA1 and PA2 in static conditions were extensively presented in a previous paper [30]. The main conclusions are summarized in the following paragraphs.

Half crystallization times for PA1 increase from approximately 400 s to 13,000 s when the crystallization temperature increased from 214 °C to 230 °C. Moreover, the lamellar growth rate G_R which was predicted by the Hoffman–Lauritzen model (Eq. (2)):

$$G_R = G_0 \exp\left(-\frac{K_g}{T\Delta T}\right)\exp\left(-\frac{U^*}{R(T-T_\infty)}\right) \quad (2)$$

with $\Delta T = T_m^0 - T$ and $T_\infty = T_g - 30$ °C.

Using the generally admitted value of U^* of 6270 J/mol [34] and the obtained values of T_m^0 (261 °C) and T_g (85 °C), both constants K_g and G_0 of Eq. (2) were obtained, respectively, 1.77×10^5 K^2 and 7.0×10^{-3} m/s. No growth regime transition was found in the investigated temperature range (219 °C–229 °C).

For PA2, the obtained half crystallization time increased from 215 s to 8700 s when the temperature increased from 218 °C to 234 °C. Moreover, for this nucleated formulation, the PA 66 crystallizes before the MXD6 whatever the crystallization conditions (isothermal or constant cooling rate).

3.2. Shear induced crystallization

The shear induced crystallization was studied thanks to the rheo-optic device for both materials. The shear rate was varied from 0.5 s^{-1} to 200 s^{-1}, and all the shearing time durations were of 5 s except for the specific study of the shearing time effect.

The results obtained for PA1 crystallization kinetics after preshear at 226 °C are shown in Fig. 2. The relative crystallinity curves are progressively shifted towards the lowest times with increasing shear rate. Half crystallization time at 226 °C decreases from 5000 s in static conditions to 930 s after a preshear of 200 s^{-1} for 5 s. Hence, the preshear treatment leads to an acceleration of the crystallization depending on the shear rate. In accordance with the literature [1,2], a critical shear rate necessary to enhance the crystallization kinetics is clearly shown in Fig. 2 since the curves for 0.5 s^{-1} and 10 s^{-1} are superimposed with the curve of static crystallization. For this material, the obtained critical shear rate is approximately of 30 s^{-1} when it is applied for 5 s in the shearing hot stage.

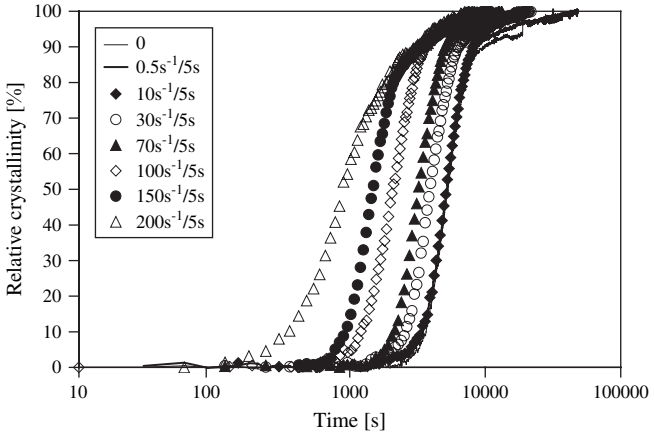

Fig. 2. Relative crystallinity curves for PA1 at 226 °C in static conditions and after different preshear treatments measured by rheo-optic device. (The experiments for 0 s^{-1}, 0.5 s^{-1} and 10 s^{-1} are superimposed.)

The effect of temperature was studied from 214 °C to 230 °C for PA1. The results will be detailed further but the general trends can be already imparted. Up to a critical shear rate, the crystallization time remains constant and then it decreases. The crystallization temperature does not seem to influence the shear effect as the decrease of the half crystallization times shows the same trend as a function of the shear rate for all the investigated temperatures. The critical shear rate value is close to 30 s^{-1} whatever the temperature.

Shear induced crystallization experiments were also performed for PA2 with a shearing time of 5 s and a shear rate varying from 0.5 s^{-1} to 200 s^{-1}. The crystallization temperature range was then from 218 °C to 234 °C. Nevertheless, for the lowest temperatures the maximum shear rates were 100 s^{-1} and 150 s^{-1} at 218 °C and 222 °C, respectively. As expected, the half crystallization times progressively decrease with increasing shear rate but the difference between the static condition crystallization and the shear induced crystallization is much lower than that observed for PA1.

To quantify the effect of shear, some acceleration ratios were defined as the ratio between the half crystallization time in static condition and the half crystallization time obtained after a preshear of 200 s^{-1}/5 s or 100 s^{-1}/5 s. These acceleration factors, respectively, a_{200} and a_{100} are shown in Table 1 for PA1 and PA2 for several temperatures. It can be noted that these factors appear mostly independent of the temperature. For PA1, a_{200} and a_{100} are close to 4.8 and 2.5, respectively. PA2 shows a lower sensibility to the shear as both values a_{200} and a_{100} are close to 2.

Table 1
Acceleration factors a_{200} and a_{100} for PA1 and PA2 at different crystallization temperatures

T [°C]	PA1		PA2	
	a_{100}	a_{200}	a_{100}	a_{200}
214	2.6	–	–	–
218	3.8	4.8	3.1	–
222	1.9	4.7	1.9	–
226	2.5	5.4	1.1	2.1
230	1.9	4.3	1.6	2
234	–	–	1.9	2.1

Furthermore, the effect of shearing time was investigated at 218 °C with PA1. The general trend of the shearing time effect is that, the half crystallization times first decreased but rapidly reached a plateau value. Hence, increasing the shearing time has only a restricted effect on the crystallization kinetics in comparison with the effect of the shear rate. Therefore, the shearing time was set to 5 s for the following experiments of the study. Indeed, this shearing time was long enough to enhance the crystallization kinetics and short enough to allow high shear rate experiments up to 200 s^{-1}. This result is consistent with the previous works [1,4,5] which also underlined a limited effect of shearing time.

Contrary to PA1 for which the effect of the shear on the crystallization kinetics is relatively important, for PA2 the applied shear rates were not sufficiently high to create a substantial accelerating effect on the crystallization process. Unfortunately, higher shear rates could not be reached experimentally. The lower sensitivity to the shear of PA2 is due to the presence of talc and PA 66, both improving its intrinsic quiescent crystallization capabilities. Indeed, the shear treatment is considered to enhance the crystallization kinetics by generating a number of activated nuclei in the sheared melt that largely exceeds the nucleation density of the quiescent unsheared melt. Therefore, when the quiescent nucleation density is high as for PA2, high shear intensities are needed to create an enhancement of the crystallization kinetics. The results are close to the conclusions of Lagasse and Maxwell [2] who studied the shear sensitivity of pure and nucleated ethylene–polypropylene copolymer (EPR). The nucleated EPR needed highest shear rates to show a significant enhancement of the crystallization kinetics. They also demonstrated that the induction times for these two materials merged for high shear rate. From a physical point of view, this merging can be explained by the following considerations: the step of the crystallization which is mainly affected by the shear is the nucleation when the shearing time is relatively short (the growth will develop after the shear). Hence, the nuclei number is increased drastically during the shear. Conversely, in quiescent conditions, the nuclei number is quite influenced by the presence or the absence of nucleating agent. Nevertheless, for high shear rates, when the nuclei number due to the shear becomes much higher than the quiescent nuclei number for both virgin and nucleated formulations, the nucleating agent becomes inefficient and the crystallization times are the same. It can be added that the higher is the nucleating agent content, the higher is the necessary shear rate to counterbalance the nucleating agent effect. Fig. 3 shows the decrease of the half crystallization times with increasing the shear rate for PA1 and PA2 at two crystallization temperatures (222 °C and 230 °C). For each temperature, the curves of PA1 and PA2 tend to converge at high shear rate. They apparently would merge for a shear rate of about 400 s^{-1}–500 s^{-1} for both temperatures. Nevertheless, experimental limitations did not allow to achieve measurements for shear rates higher than 200 s^{-1}. Thus, this merging could not be experimentally established.

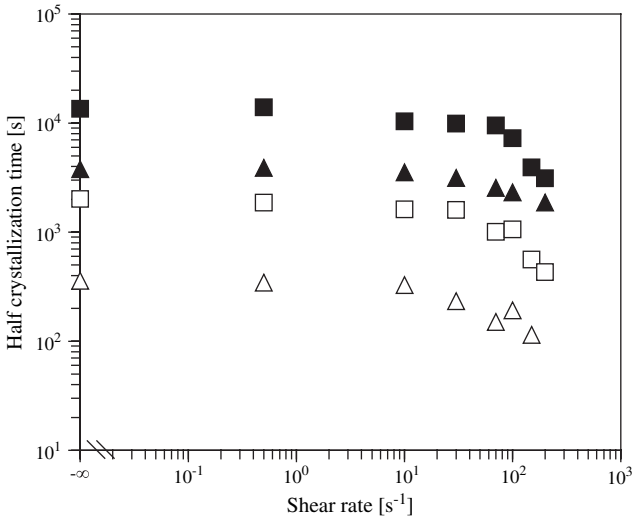

Fig. 3. Crystallization characteristic times versus shear rate (shearing time 5 s) for PA1 at 222 °C (□), PA1 at 230 °C (■), PA2 (△) at 222 °C and PA2 at 230 °C (▲).

3.3. Kinetic model

A kinetic model was previously developed to describe the quiescent crystallization results [30] for the virgin and nucleated formulations taking into account the temperature effect. In the present work the model is extended including the shear induced crystallization for both PA1 and PA2. The basic model, for quiescent conditions, was based on a combination of the Avrami and the Hoffman–Lauritzen equations where the effect of temperature was introduced using the expression of the growth rate (Eq. (2)) and a variation of the nuclei number with temperature, this later variation being different for PA1 (virgin) and PA2 (with nucleating additives). Moreover, it was concluded that considering an instantaneous nucleation was suitable so that the Avrami exponent n was set to 3. Furthermore, it was shown that the growth rate could be considered unchanged in the presence of nucleating agents which affects only the nuclei number in PA2. The basic additional assumptions necessary to account for the shear effect are, (i) that the lamellae growth rate G_R does not depend on the shear rate as it is generally admitted for shear treatments which are relatively short compared to the whole crystallization times [5,7,11] and, (ii) that the shear affects only the nucleation rate in the melt. Therefore, the expanded transformed volume fraction α' is modified to take into account the number of nuclei due to the preshear:

$$\alpha'(t) = \frac{4}{3}\pi G_R^3 \left[N_0 t^3 + \int_0^{t_s} (t-t')^3 \dot{N}(t') \mathrm{d}t' \right] \tag{3}$$

where N_0 is the natural nuclei number per unit volume in the quiescent melt, $\dot{N}(t)$ the nucleation rate and t_s the shearing time. The relative crystallinity (α) takes into account the fact that the spherulites impinge during the crystallization and is written as:

$$\alpha = 1 - \exp(-\alpha') \tag{4}$$

According to different previous works [5,35], the natural nuclei number in quiescent melt N_0 was expressed as a function of the supercooling $\Delta T = T_m^0 - T$:

$$N_0 = \exp(a\Delta T + b) \tag{5}$$

The parameters a and b were fitted on the experimental half crystallization times obtained in static isothermal crystallization as detailed in the previous paper [30]. Their values are summarized in Table 2 where the calculated values of the nuclei number per unit volume N_0 for the temperatures of 218 °C and 230 °C are also reported.

It can be noticed that, as expected, Eq. (3) is reduced to the classical Avrami equation (Eq. (6)) with instantaneous nucleation ($n = 3$) for zero shear.

$$\alpha = 1 - \exp(-K_{\mathrm{Avrami}} t^n) \text{ with } K_{\mathrm{Avrami}} = \frac{4}{3}\pi N_0 G_R^3 \tag{6}$$

Finally, the nucleation rate $\dot{N}(t)$ appearing in Eq. (3) must be expressed as a function of the shear rate. In this respect, several expressions can be found in the literature with the $\dot{N}(t)$ proportional to a power law of the shear rate. The used exponents for this power law can vary from 1 [7] to 2 or 4 [10]. More recently Janeschitz-Kriegl et al. [36,37] linked the nuclei number to the mechanical work provided by the shear treatment to the material. They obtained a power law with an exponent between 2 and 3. Then, recalling that the mechanical work for a constant shear rate can be evaluated by $\eta\dot{\gamma}^2 t_s$, it turns out that the nuclei number, and therefore the nucleation rate, can be represented by a power law of the shear rate with an exponent between 4 and 6. Thus, according to the literature, in the present work, the nucleation rate was expressed by a semi-empirical power function of the shear rate $\dot{\gamma}$.

$$\dot{N}(t') = \left[c\dot{\gamma}(t') \right]^d \tag{7}$$

The combination of Eqs. (3), (4) and (6) allows to express the relation between the relative crystallinity α and the

Table 2
Values of parameters a, b, c and d for PA1 and PA2 kinetic models and nuclei number N_0 as a function of the temperature

	a	b	c [s$^{2/3}$ m^{-1}]	d	N_0 [m^{-3}] $T = 218$ °C	N_0 [m^{-3}] $T = 230$ °C
PA1	6.09×10^{-2}	29.08	6.267×10^2	3	5.8×10^{13}	2.8×10^{13}
PA2	2.63×10^{-1}	26.82	6.267×10^2	3	3.7×10^{16}	1.6×10^{15}

corresponding time. Moreover, the integral of Eq. (3) can be analytically calculated. Hence Eq. (8) is deduced:

$$\alpha' = \ln\left(\frac{1}{1-\alpha}\right) = \frac{4}{3}\pi G_R^3\left[N_0 t_\alpha^3 + c\dot{\gamma}^d\left(t_s t_\alpha^3 - \frac{3}{2}t_s^2 t_\alpha^2 + t_s^3 t_\alpha - \frac{t_s^4}{4}\right)\right] \quad (8)$$

where t_α is the time corresponding to a given value of α.

Therefore, the time for any relative crystallinity value can be extracted by resolving the third degree equation (Eq. (8)). The remaining unknown parameters (c and d) were numerically optimized to fit the decrease of the half crystallization times ($t_{1/2}$) with increasing the shear rate. These parameters appeared independent of the temperature and the obtained values are reported in Table 2. First, in Fig. 4, the relative crystallinity curves for one temperature (226 °C) and different shear rates are plotted (shearing time 5 s) comparing experimental data with the calculated ones. As it is shown, the model is able to well predict the crystallization kinetics and the shear effect, especially for the first part of the crystallization. However, at the end of the crystallization, the slowing shown by the experimental curves and due to secondary crystallization is not forecasted by the model. Moreover, data for PA1 are gathered in Fig. 5 in terms of half crystallization times versus the shear rate for different temperatures. Globally these data are well represented by the model. Particularly, the model prediction exhibits a critical shear rate (at approximately 30 s^{-1}) which corresponds to the experimental data. It can be specified that the critical shear rate is predicted by the model via the balance between the first and the second terms in the bracket of Eq. (3). Indeed, the critical shear rate is reached when the second term which contains the shear effect becomes greater than the first one which accounts for the natural nucleation. Moreover, the slope of the curve for a shear rate higher than the critical one is governed mainly by the exponent d in Eq. (7).

Fig. 6 shows the comparison between the experimental and calculated results for PA2. Again, the model prediction appears consistent with the experiments except at 234 °C where

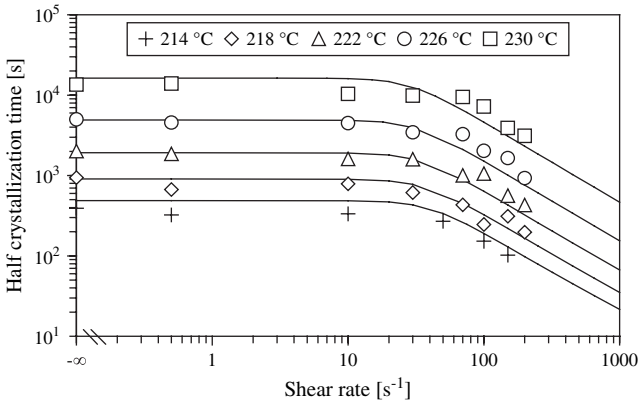

Fig. 5. Experimental (symbols) and predicted (lines) half crystallization times versus shear rate for PA1 for different temperatures (shearing time 5 s).

the half crystallization times are overestimated. This discrepancy probably originates from the evaluation of the growth rate by Eq. (2) at 234 °C. Indeed, this temperature is higher than the temperature range where the parameters of Eq. (2) were determined (219 °C–229 °C) and the extrapolation to 234 °C may be unsuitable because of a growth regime transition between 229 °C and 234 °C.

Moreover, because of the talc and the PA 66 which crystallizes before the MXD6, it could be pointed out that the effective shear undergone by the MXD6 is higher than the nominal one. Actually, in our approach, the effective shear rate was considered equivalent to the nominal one. Indeed, the effect of the non-deformable talc was neglected since its amount is only 1% by weight (that is even much less by volume). As concerns the PA 66 (11%), obviously its amount cannot be neglected. Though, it was shown by rheological measurements in the previous paper [30], that the crystallization of the PA 66 in the MXD6 in this temperature range leads to a kind of very weak network which confers a certain elasticity to the material. Moreover, when a continuous shear is applied to the material, the elasticity disappears and takes a certain time to be recovered. Hence, it can be deduced that the PA 66 and MXD6 are miscible in the melt state. In other words, more

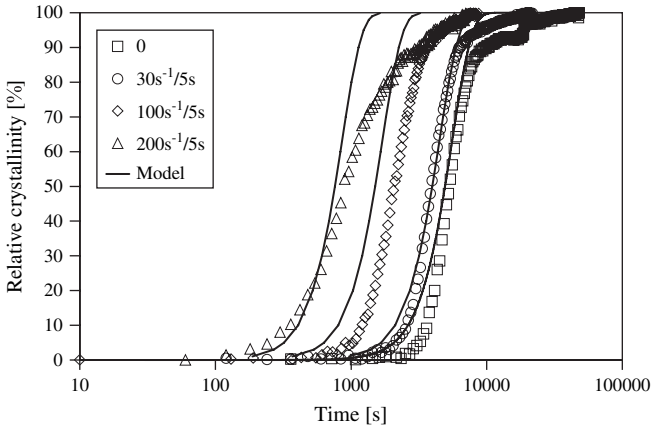

Fig. 4. Relative crystallinity curves for PA1 at 226 °C for different shear rates (shearing time 5 s). Symbols: experimental data, lines: calculated curves.

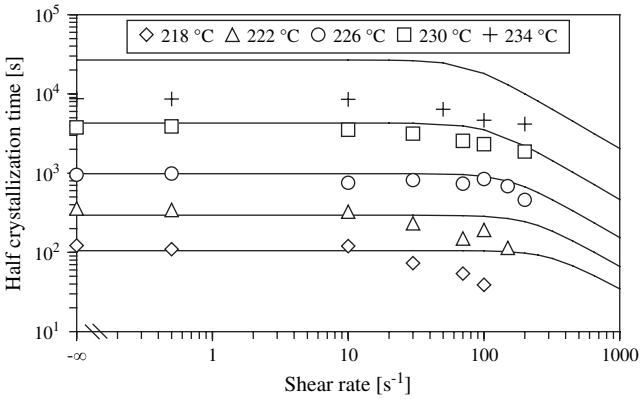

Fig. 6. Experimental (symbols) and predicted (lines) half crystallization times versus shear rate for PA2 for different temperatures (shearing time 5 s).

than effective solid particles dispersed in the matrix, the crystallized PA 66 can be considered as very weak physical gel which is destroyed during the shear. As a conclusion, even if the PA 66 crystallizes faster than the MXD6, it probably does not perturb the shear of the MXD6. Therefore, the effective shear rate can be assimilated to the nominal one.

One of the other interesting issues is that even if lot of parameters are temperature dependent (quiescent nuclei number, growth rate, rheological behavior), it appears that the critical shear rate itself does not greatly depend on temperature (see Fig. 5). This apparently paradoxical result may be explained as follows: the temperature dependence of the quiescent nucleation rate is very important, in the present temperature range (214 °C–230 °C). Comparatively, the rheological behavior does not change a lot in a so narrow temperature range. Thus, the molecular orientation for a given shearing, and consequently the nucleation rate are not strongly temperature dependent. Besides Eq. (7) used for the nucleation rate due to the shear does not include any temperature dependence. On the other hand, the effect of the shear rate on the nucleation is very high (shear rate to the power 3 in Eq. (7)), so high that the nuclei number due to the shear becomes greater than the quiescent nuclei number for practically the same shear rate in the studied temperature range. In other words, the global nuclei number is more dependent on the shear rate, when it is sufficient, than on the temperature.

It could be added that if the calculated curves in Figs. 5 and 6 were plotted in a same plot (not shown here), for each temperature, they would become unique at high shear rate for both formulations as expected (see previous discussion concerning the merging of data for nucleated and virgin formulation).

Finally, the model was also used to describe the effect of shearing time which was measured for PA1 at 218 °C. As highlighted in Fig. 7, the shearing time effect is also well predicted by the model.

As a result, the proposed model that is based on simple but reasonable assumptions appears suitable to describe several features of the crystallization kinetics of the studied PAs. Particularly, it can predict the effect of the temperature, the formulation (with or without nucleating additives) and especially the effect of shear, while preserving a small number of adjustable parameters. Nevertheless, this model is not able to predict the crystalline morphology and orientation developed because of shear.

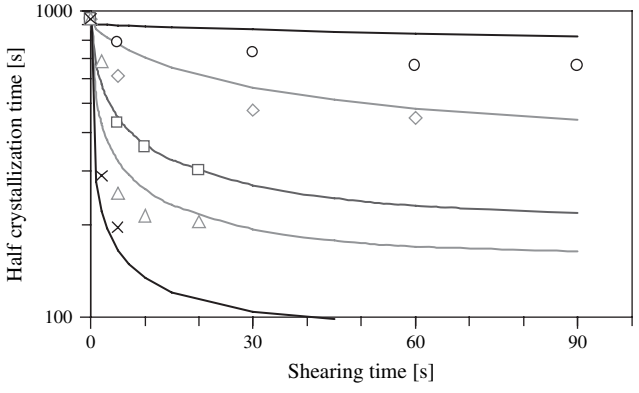

Fig. 7. Experimental (symbols) and predicted (lines) half crystallization times versus shearing time for PA1 at 218 °C for different shear rates. ○: 10 s^{-1}; ◇: 30 s^{-1}; □: 70 s^{-1}; △: 100 s^{-1}; ×: 200 s^{-1}.

3.4. Crystalline morphology study

3.4.1. Crystalline cell orientations

WAXD experiments were performed on both materials crystallized in the rheometer at 226 °C after a shear of 200 s^{-1} for 5 s following the procedure exposed in the experimental part. Samples were positioned flat on the rotating support with the shear direction initially parallel to the X-ray beam. Samples were progressively rotated around the axis normal to the sample (*i.e.* to the shear plane) with steps of 9°. Nevertheless, for both PAs, the rotation did not lead to a significant change which indicates that the crystalline orientation shows a cylindrical symmetry around the normal axis. Therefore, the results will only be shown for an X-ray beam parallel to the shear direction.

Fig. 8 shows the diffraction pattern for PA1 (a) and PA2 (b). For PA1, two main diffraction rings corresponding to the interplanar distances of 0.472 nm and 0.417 nm are obtained. According to the works of Ota et al. [27] and the highest structural factors of planes of the MXD6 triclinic cell, these rings were attributed, respectively, to the (100) planes and to the (010) and (110) crystalline planes whose interplanar distances are so close that they could not be distinguished in this study ($d_{010} = 0.417$ nm and $d_{110} = 0.419$ nm).

Additionally to the diffraction rings due to MXD6, the diffraction pattern of PA2 showed also two well-defined diffraction rings corresponding to interplanar distances of about 0.940 nm and 0.310 nm. They were attributed to the (002) and (006) reflections of talc which presents a monoclinic cell whose parameters are $a = 0.526$ nm; $b = 0.910$ nm; $c = 1.881$ nm; $\alpha = \gamma = 90°$; and $\beta = 100°$ [38,39]. It should be noted that for talc, the (004) crystalline plane should lead to a diffraction peak. However, the interplanar distance is $d_{004} = 0.470$ nm so that this ring is embedded in the diffraction ring due to the (100) planes of MXD6 crystal. Additionally, some diffraction peaks of lower intensity, obtained in the diffraction pattern of PA2, can be attributed to the PA 66 crystals of triclinic cell with the following parameters: $a = 0.49$ nm; $b = 0.54$ nm; $c = 1.72$ nm; $\alpha = 48.5°$; $\beta = 77°$; and $\gamma = 63.5°$ [40]. These PA 66 rings correspond to the (010) and (110) planes of interplanar distance close to 0.37 nm and the (002) planes of distance close to 0.64 nm.

The different indexations are summarized in Fig. 9 which shows the diffraction results for two azimuthal angles for the PA2 sheared at 200 s^{-1} for 5 s. Actually, this corresponds to the plots of the recorded intensity along two radii of Fig. 8b (horizontal: $\varphi = 0°$ and vertical: $\varphi = 90°$). For comparison, the inset in Fig. 9 shows the intensity for the same azimuthal angles of PA2 crystallized without shear revealing no orientation, as expected.

Furthermore, both Figs. 8 and 9 reveal some orientation by the variation of the intensity along the diffraction rings, as

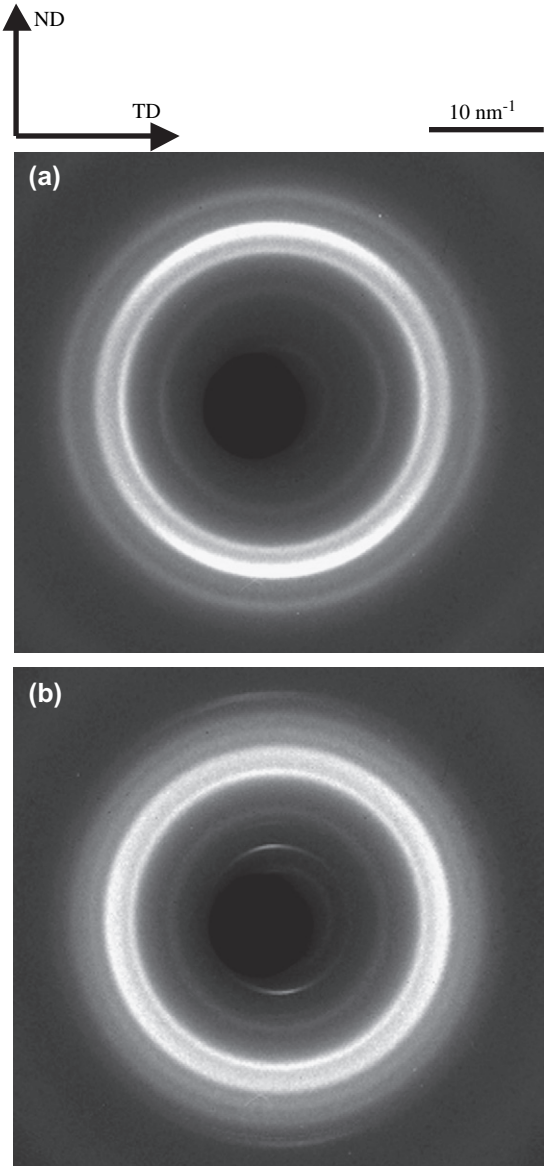

Fig. 8. Diffraction patterns of PA1 (a) and PA2 (b) crystallized at 226 °C after a preshear of 200 s^{-1} for 5 s. X-ray beam is parallel to the shear direction, SD: shearing direction, ND: direction normal to the shear plane.

a function of the azimuthal angle. This feature is highlighted by Fig. 10 for PA1 and Fig. 11 for PA2 where the intensity diffracted by the (100) planes and by both (010) and (110) planes are plotted versus the azimuthal angle. Moreover, from these two Figures, it can be clearly seen that (i), the crystalline orientation is much more pronounced in the PA1 sample and (ii), the crystalline orientation is different in PA1 and PA2.

First, for PA1 (Fig. 10), the diffraction due to the (010) and (110) planes is largely higher for an azimuthal angle at about 90°. Moreover, as already mentioned, the rotation of the sample around to its normal direction did not significantly change the diffraction patterns. Therefore, even if more experiments should be necessary to rigorously determine the main orientation of the unit cell, it can be concluded that the (010) and (110) planes are preferentially aligned in the shear plane. Indeed, because of shear, it can be foreseen that the macromolecular chains could be oriented in the shear plane (but not necessary in the shear direction) with the benzene rings also oriented in the shear plane. In the crystalline cell, these benzene rings are in the (120) plane [27] which forms an angle of 26.4° with the (110) plane and an angle of 26.3° with the (010) plane. Unfortunately it was not possible to detect the diffraction of these (120) planes because the corresponding structure factor is relatively low. However, this assumption could be supported by the fact that the (010) and (110) planes diffraction intensity is higher for an azimuthal angle centered at 90° but spreading over a relatively broad angle range (±26°). In Fig. 12, the proposed crystalline cell orientation is plotted for the virgin grade (PA1). In this figure, the curved arrow indicates the possible cylindrical symmetry deduced from the quasi invariance of the pattern when rotating the sample around the normal to the shear plane.

Concerning the nucleated grade, Fig. 11 highlights the slight crystalline preferential orientation observed in PA2 sheared sample. The low orientation level is to be linked to crystallization kinetics. Indeed the sample was sheared at 226 °C for 5 s at 200 s^{-1} and, as it can be seen in Fig. 6, this shear treatment does not considerably decrease the crystallization time of the nucleated grade. In other words, the crystallization occurs practically as for shear free conditions. Thus, considering that the crystalline orientation would result of the orientation of the shear induced nuclei, a low resulting orientation level is expected when the shear rate is lower than the critical shear rate necessary to enhance the crystallization kinetics. For comparison, the PA1 grade exhibited a greater orientation linked to the high effect of the shear treatment on the crystallization kinetics (see Fig. 5) indicating a high number of oriented nuclei due to the shear.

Nevertheless, even if the orientation level is low for PA2, Figs. 9 and 11 show that this crystalline orientation is actually present and, as already noted, it is not the same as it was for PA1. Indeed, the (100) planes of MXD6 crystal now preferentially diffract the X-rays for an azimuthal angle of about 90° whereas the (010) and (110) planes preferentially diffract around 0° but more precisely between −26° and +26°. It should be added that even if the diffraction ring of (004) plane of the talc crystal overlaps with the diffraction ring due to (100) planes of MXD6 crystal (see Fig. 9), the diffraction ring corresponding to (010) and (110) planes is not altered by the talc nor by the PA 66. Thus the variation of its intensity with the azimuthal angle is really due to MXD6 preferential orientation. Besides, likewise for PA1, the rotation of the PA2 sample around the normal of the shear plane did not significantly change the diffraction patterns so that again, a cylindrical symmetry of the crystalline orientation is expected. Moreover, as it can be seen in Fig. 8b and in Fig. 9, the talc crystalline planes (002) and (006) diffract at an azimuthal angle of 90°, hence revealing a noticeable preferential orientation of the talc platelets in the shear plane, consistently with literature data [41–45]. The preferential orientations of MXD6 and talc crystals in PA2 are, respectively, shown in Fig. 13a and b. Again, the proposed preferential orientation for MXD6 crystals corresponds to the macromolecular

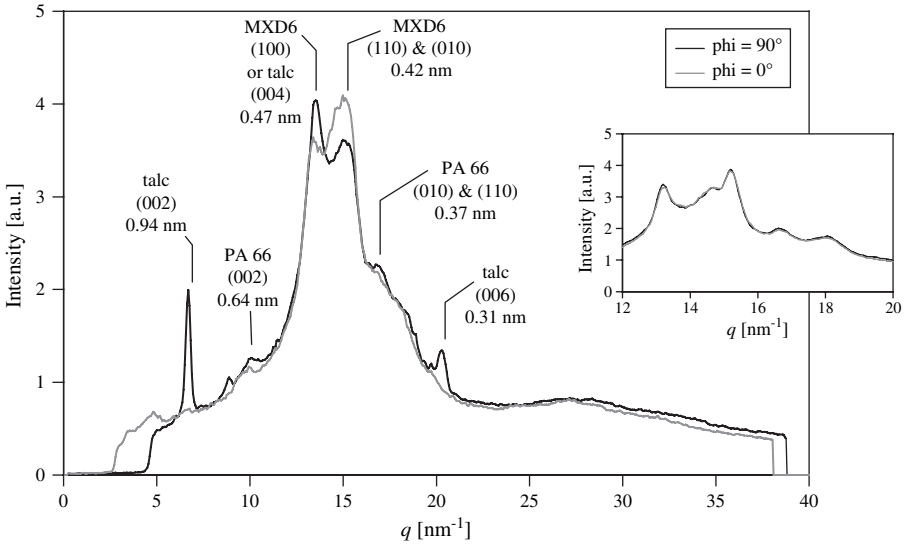

Fig. 9. Diffractograms for two azimuthal angles of PA2 crystallized at 226 °C after a preshear of 200 s^{-1} for 5 s. The diffraction planes of MXD6, PA 66 and talc are indicated with their respective interplanar distances. X-ray beam is parallel to the shear direction (inset: diffractograms of PA2 crystallized without shear).

backbone in the shear plane, but, contrary to the case of the virgin grade, the (120) plane containing the benzene rings is now perpendicular to the shear plane. Obviously, it can be foreseen that the PA 66 crystals may be oriented as well but it was not possible to correctly investigate this feature in the present study because of the low diffraction intensity for PA 66 (see Fig. 9). Nevertheless, this eventual orientation of PA 66 is probably not very important (similarly to the MXD6 orientation in PA2) because, as it was already mentioned, the crystallization kinetics is not considerably enhanced for the present shear treatment.

Since in this case of PA2, the crystallization of MXD6 is mainly induced by the nucleating additives (talc and/or PA 66), the orientation of MXD6 crystal may be governed by the orientation of these additives. Thus, the difference of preferential orientation between the virgin and the nucleated grades may be explained as follows: for the virgin grade, the shear directly orients the backbone and the benzene rings in the shear plane. Conversely, in the presence of the talc and the PA 66, the MXD6 crystals orientation will be different since it is a consequence of the previous orientation of the talc platelets or the PA 66 crystals. If the MXD6 crystals originates from the talc, it would lead to transcrystalline layers on talc particles as it was already reported in the works of Naiki et al. [43] and Choi et al. [45] for injected samples of talc nucleated polypropylene. According to this point of view, it can be added that the crystalline orientation of MXD6 in PA2 could be determined as a result of epitaxial growth on (001) plane of the pre-oriented talc crystal. Indeed, the lattice spacing of (040) and (220) planes of talc are 0.228 nm and 0.225 nm, respectively. Because the lattice spacing of (120) plane of MXD6 is 0.233 nm, lattice matching is possible. On the other hand, if the MXD6 crystals rather originate from the PA 66, the orientation should be much less pronounced since the PA 66 crystals are likely not to be noticeably oriented. Therefore, in the present case where the orientation of MXD6 remains weak, it seems that the nucleation of MXD6 crystals is rather induced by the PA 66.

As a conclusion, it can be added that the orientation of MXD6 as shown in Fig. 13a should be obtained only for

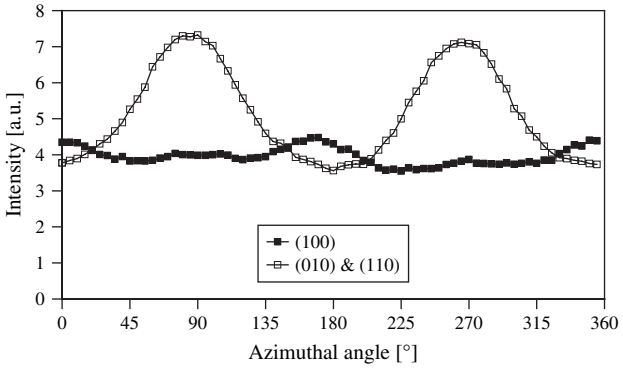

Fig. 10. Intensity of the two main diffraction peaks versus azimuthal angle for the PA1 crystallized at 226 °C after a preshear of 200 s^{-1} for 5 s.

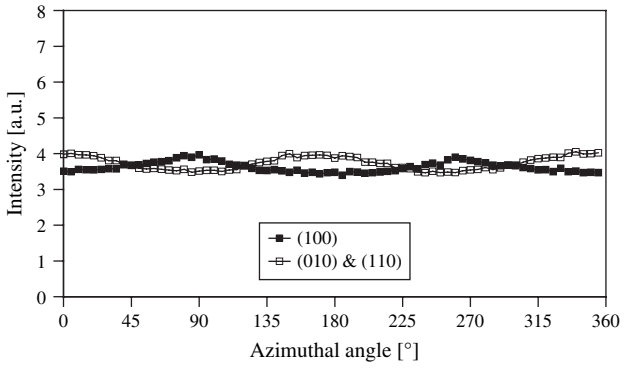

Fig. 11. Intensity of the two main diffraction peaks versus azimuthal angle for the PA2 crystallized at 226 °C after a preshear of 200 s^{-1} for 5 s.

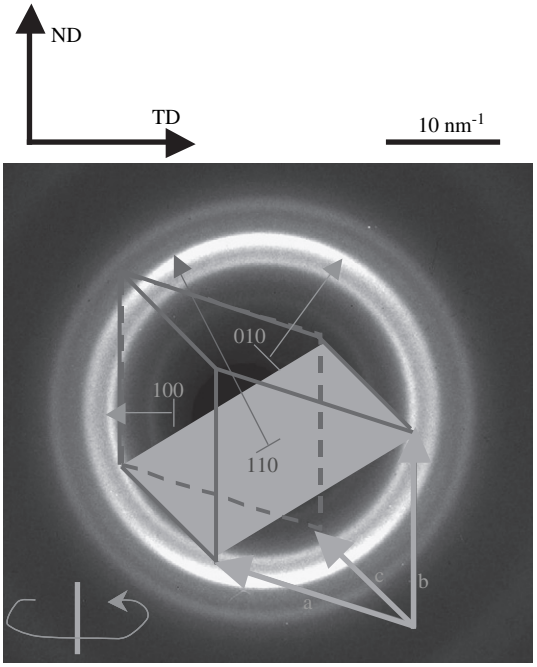

Fig. 12. Possible preferential position of the MXD6 crystal cell in a sheared sample of PA1. The small arrows indicate the preferential diffraction direction of the planes. The curved arrow indicates the cylindrical symmetry. X-ray beam is parallel to the shear direction, ND: direction normal to the shear plane, TD: direction in the shear plane, perpendicular to the shear direction.

moderated shear treatments. Indeed, when the shear treatment would become sufficient to enhance the crystallization kinetics, that is to say, to provide shear induced nuclei more numerous than the nuclei due to the nucleating additives, the orientation should be the same as for the virgin grade (Fig. 12).

3.4.2. Crystalline lamellae analysis

SAXS measurements were performed on samples of PA1 and PA2, both crystallized at 226 °C after a preshear of 200 s^{-1} for 5 s. Fig. 14a–d shows the scattering patterns for both samples and for X-ray beam normal to the shear plane and in the shear plane but perpendicular to the shear direction. Moreover, Fig. 15 shows the plot of the intensity as a function of the scattering vector q for an azimuthal angle of 0° in Fig. 14b and d. The first conclusion deals with the nucleating agents and more particularly the talc platelets. In the presence of these fillers, the scattering intensity for PA2 is considerably higher than in PA1 (see Fig. 15), likely because of talc. Moreover, the scattering intensity due to the talc is so high that the scattering of the MXD6 crystalline lamellae in PA2 is practically undetectable (no correlation peak). Furthermore, as shown by the scattering pattern in Fig. 14c the talc platelets are oriented in the shear plane as already shown by the WAXD analysis.

Contrary to PA2, the PA1 scattering patterns show a well defined maximum typical of a semi-crystalline lamellar system as illustrated in Fig. 15. This correlation peak is located at a scattering vector value $q = 0.5\ nm^{-1}$. The long period (Lp) can be determined by two different ways [35,46]. First,

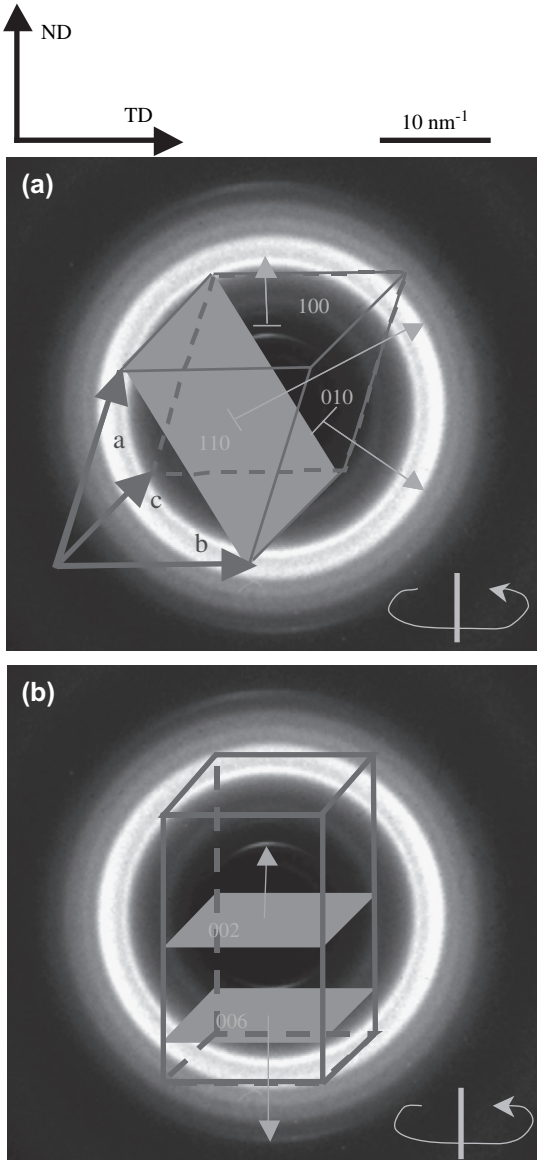

Fig. 13. Possible preferential positions of the crystal cells in a sheared sample of PA2. (a) MXD6 triclinic cell, (b) talc monoclinic cell. The small arrows indicate the preferential diffraction direction of the planes. The curved arrow indicates the cylindrical symmetry. X-ray beam is parallel to the shear direction. ND: direction normal to the shear plane, TD: direction in the shear plane, perpendicular to the shear direction.

the position q_{max} of the maximum of the Lorentz-corrected intensity $I_1(q) = q^2 I(q)$ was calculated. Then Lp can be deduced from:

$$Lp = \frac{2\pi}{q_{max}} \tag{9}$$

With this method, the obtained value of q_{max} was 0.54 nm^{-1} so that Lp = 11.6 nm.

The second method used consisted in the calculation of the autocorrelation function $\Gamma(r)$ from the cosine Fourier transform of $q^2 I(q)$:

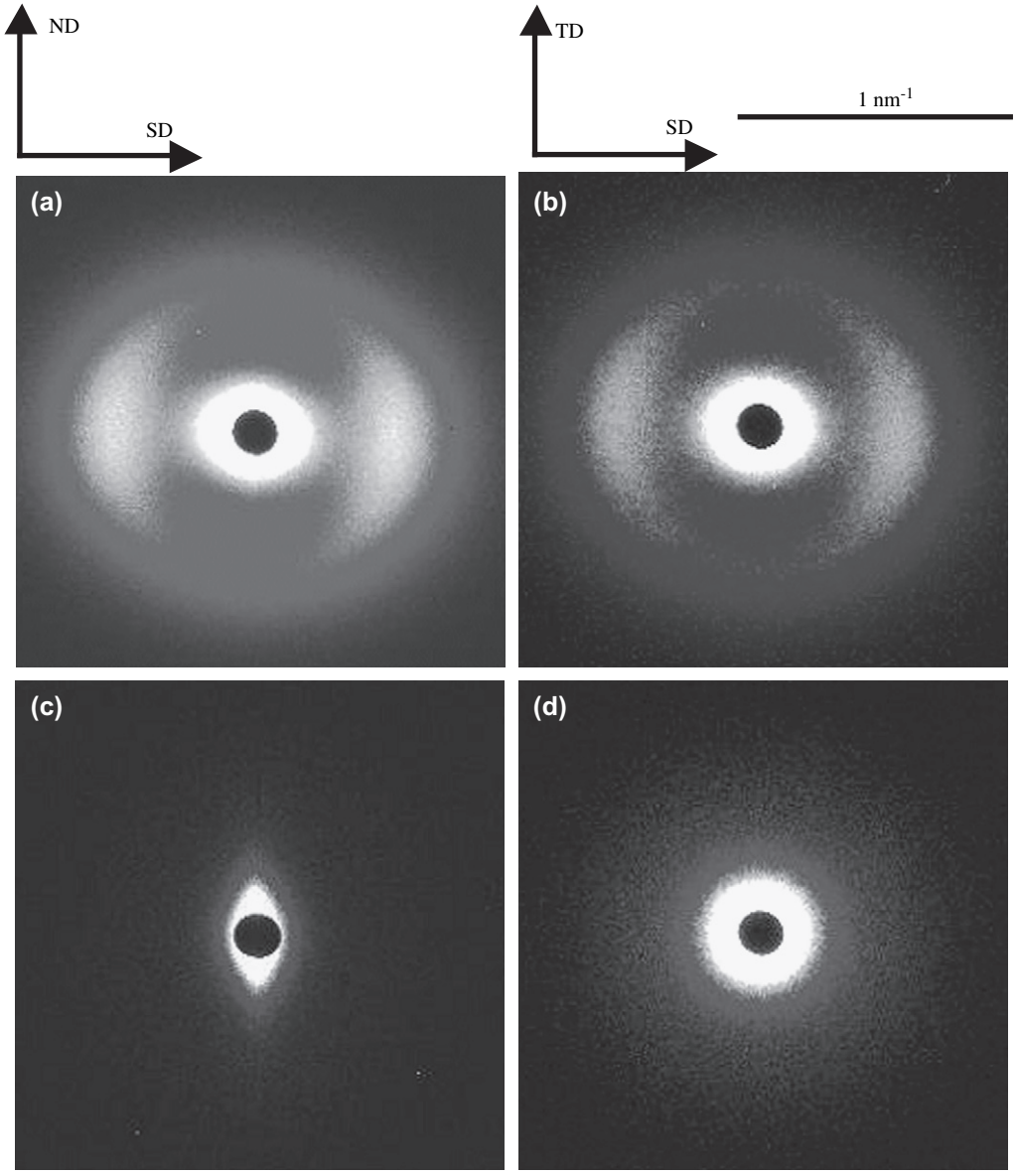

Fig. 14. Scattering patterns for PA1 (a and b) and PA2 (c and d). SD: shearing direction, ND: direction normal to the shear plane, TD: direction in the shear plane, perpendicular to the shear direction. Patterns (a) and (c): X-ray beam is parallel to TD. Patterns (b) and (d): X-ray beam is parallel to ND.

$$\Gamma(r) = \frac{\int_0^{+\infty} q^2 I(q)\cos(qr)\mathrm{d}q}{\int_0^{+\infty} q^2 I(q)\mathrm{d}q} \tag{10}$$

In order to calculate the integrals defined above, extrapolations of the data for the small q and for the large q ranges were necessary. At low q the power law $I(q) = aq^{\phi}$ was used and the Porod's asymptote $I(q) = C/q^4 + B/q^2$ was used for the large q range. The first maximum of the correlation function $\Gamma(r)$ finally yields the long period. In all cases, the values deduced by both methods are in good agreement: Lp = 11.5 nm ($\phi = 1.85$; $a = 1.747 \times 10^6\ \mathrm{nm}^{1.85}$; $B = 2.705 \times 10^4\ \mathrm{nm}^{-2}$; $C = 2.207 \times 10^4\ \mathrm{nm}^{-4}$).

Moreover, from the correlation function, the thickness of the crystalline and amorphous lamellae can be evaluated, provided that the value of the crystallinity is available [46]. From previous data [30] concerning the same materials, the estimated crystallinity of MXD6 was lower than 24% in all cases. Different alternative methods have been proposed in literature for deducing the lamellae thickness. One of them consists in determining the abscissa (l) of the intercept between the tangent of the correlation function at the origin and the horizontal line which passes through its first minimum. From the correlation function the obtained value of l was 2.3 nm. The ambiguity to assign this size to the crystalline or the amorphous lamella thickness is resolved thanks to the low obtained crystallinity and this leads to a crystalline lamella thickness l_c of 2.3 nm and an amorphous lamella thickness of 9.2 nm ($l_a = \mathrm{Lp} - l_c$).

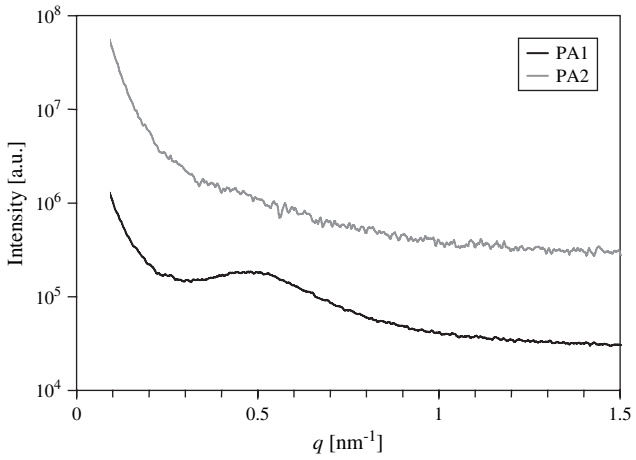

Fig. 15. Scattering intensity versus the scattering vector for PA1 and PA2 samples crystallized at 226 °C after a preshear of 200 s^{-1} for 5 s. The plot corresponds to an azimuthal angle of 0° (horizontal) in Fig. 14b and d.

The 2D SAXS patterns of PA1 can also provide some details concerning the crystalline lamellae orientation. From Fig. 14a and b, it can be observed that the lamellae appears preferentially perpendicular to the shear plane. Indeed, the scattered intensity maximum appears at an azimuthal angle of 0° for both these patterns, indicating that the stack periodicity (*i.e.* the small dimension direction of the lamellae) is parallel to the shear direction. Surprisingly, this result only partially agrees with the conclusions drawn from WAXD experiments. Indeed, from WAXD, it was concluded that the macromolecular backbone of the MXD6 chains were aligned in the shear plane with the benzene rings oriented also in the shear plane and this first main conclusion is corroborated by the SAXS. However, the fact that the WAXD patterns are not modified by the rotation of the sample around the normal to the shear plane allows to conclude that there was a cylindrical symmetry of the orientation around this axis. Consequently all orientations of the crystalline lamellae with the thickness direction in the shear plane could be possible. This last result slightly differs from the SAXS data which indicate rather a preferential orientation of the lamellae with their normal direction parallel to the shear direction. Obviously, more investigations should be performed to unquestionably remove this discrepancy but at this stage, it could be deduced that there is a slight preferential orientation of the lamellar thickness direction parallel to the shear direction, as revealed by SAXS experiments, this orientation being not sufficient to be revealed by WAXD.

3.4.3. Crystalline orientation versus kinetic model

A comment can be added concerning the links between the crystallization kinetics and the obtained crystalline orientation. Indeed, for the considered shear treatment (200 s^{-1} for 5 s at 226 °C), the crystalline orientation is important for PA1 and low for PA2. Moreover, from a kinetic point of view, the enhancement due to this shear treatment is more efficient for PA1 than for PA2 (see for example Table 2). Additionally, the kinetic enhancement being considered as a result of the increasing nucleation due to the molecular orientation by the shear, it follows that the kinetic enhancement should coincide with a resulting crystalline orientation. Nevertheless, it must be recalled that, in the presented kinetic model, a non-oriented spherulitic structure was considered to calculate the expanded volume (see Eq. (3)). Obviously, this is one of the drawbacks of the presented kinetic model which is inadequate to predict any crystalline orientation. One of the ways of its improvement should be in revisiting Eq. (3) to take into account the development of non-spherical entities. However, this would lead to a more complex model required to determine more parameters. Nevertheless, from a merely kinetic point of view, the model introduced in the present work remains reliable in predicting the crystallization times.

4. Conclusion

The present study showed the enhancing effect of shear on the crystallization kinetics of the MXD6 for both virgin or nucleated grades. For a constant shearing time, and for shear rates higher than a critical value, the enhancement of the crystallization kinetics increases with increasing the shear rate, as it has been observed for many polymers. For a definite shear rate, increasing the shearing time leads also to enhance the crystallization kinetics but only up to a given level that is reached asymptotically. Moreover, in the investigated temperature range, the crystallization temperature does not affect the shear effect on the crystallization kinetics. Besides, the virgin grade of MXD6 is more sensitive to the shear with a lower critical shear rate and a more important decrease of the crystallization time than for the nucleated grade. That can be explained by the creation of additional nuclei with chain alignment induced by shear. Thus, the shear can be efficient only if the shear induced nuclei become more numerous than in the quiescent melt. Obviously, in the nucleated grade of MXD6, the quiescent nuclei number is higher than in the virgin grade, so that it requires a higher number of shear induced nuclei and thus, a stronger shear treatment to change the crystallization kinetics.

From these observations, a simple kinetic model based on the Avrami equation has been proposed in order to take into account separately the different parameters. First, based on previous analyses [30], the temperature effect was introduced including the effect on the growth rate and on the quiescent nuclei number which is obviously also affected by nucleating agents. Second, the shear effect was introduced by relating the additional nucleation frequency to the shear rate by an empirical power law which leads to a good prediction of the effect of both the shear rate and the shearing time and for both formulations.

Moreover, X-ray analyses provided a microstructural description of the shear effects. In identical shear conditions, the non-nucleated grade exhibits a more pronounced orientation than the nucleated one, in good agreement with the previous conclusion that the shear is more efficient for the non-nucleated polymer. Indeed, it seems that these specific

shearing conditions are not enough strong to largely enhance the crystallization kinetics of the nucleated polymer and consequently to largely orient the resulting crystalline morphology. Moreover, the obtained crystalline orientation is different between the virgin and the nucleated grades. Indeed for the virgin polymer, the main crystalline orientation appears to be with the chain backbone and the benzene rings parallel to the shear plane. Alternatively, for the nucleated grade, the weak crystalline orientation appears with the chain backbone still in the shear plane but with the benzene rings perpendicular to the shear plane, possibly because of a heterogeneous nucleation on the nucleating agents which are themselves oriented in the shear plane. This result is consistent with the low effect of shear on the MXD6 crystallization in the nucleated grade, otherwise the orientation would be the same than in the virgin grade. Indeed, for the nucleated grade, the shear affects the orientation of the talc platelets but, as mentioned before, if the shear was really efficient in directly enhancing the crystallization kinetics, this would be due to a large number of nuclei generated by the chain orientation independently of the nucleating agent. In that case, the resulting crystalline orientation should be the same than for the virgin grade.

The last conclusion may be extrapolated to practical applications. For example, if one would like to govern the crystalline orientation by adding some nucleating agents of high shape ratio and expecting them to be oriented by the processing to determine the subsequent crystalline orientation, one would be careful that the shear due to the processing is not too strong otherwise the nucleating agent efficiency will be lost. On the other hand one may compensate this shear effect by adding more nucleating agent.

Acknowledgments

We would like to acknowledge gratefully the companies Legrand, Solvay and Moldflow for financial support, material supply and characterization. We would like to thank more particularly Peter Kennedy, Rong Zheng, Hugues Alglave, Vito Leo, Florentin Langouche, Michel Laplanche, Jean-Michel Rossignol, Joachim Correa, Gilles Regnier, Didier Delaunay, Delphine Dray and Ronan Legoff for stimulating discussions. Moreover we would like to thank the French CRG beamline D2AM for the X-ray measurements.

References

[1] Tribout C, Monasse B, Haudin JM. Colloid Polym Sci 1996;274(3):197–208.
[2] Lagasse RR, Maxwell B. Polym Eng Sci 1976;16(3):189–99.
[3] Haas TW, Maxwell B. Polym Eng Sci 1969;9(4):225–41.
[4] Kumaraswamy G, Issian AM, Kornfield JA. Macromolecules 1999;32:7537–47.
[5] Koscher E, Fulchiron R. Polymer 2002;43(25):6931–42.
[6] Jay F, Haudin JM, Monasse B. J Mater Sci 1999;34:2089–102.
[7] Wolkowicz MD. J Polym Sci Polym Symp 1978;63:365–82.
[8] Lellinger D, Floudas G, Alig I. Polymer 2003;44:5759–69.
[9] Masubuchi Y, Watanabe K, Nagatake W, Takimoto JI, Koyama K. Polymer 2001;42:5023–7.
[10] Liedauer S, Eder G, Janeschitz-Kriegl H, Jerschow P, Geymayer W, Ingolic E. Int Polym Process 1993;VIII:236–44.
[11] Abuzaina FM, Fitz BD, Andjelic S, Jamiolkowski DD. Polymer 2002;43:4699–708.
[12] Avrami M. J Chem Phys 1939;7:1103–12.
[13] Avrami M. J Chem Phys 1940;8:212–24.
[14] Avrami M. J Chem Phys 1941;9:177–84.
[15] Ozawa T. Polymer 1971;12:150–78.
[16] Nakamura K, Watanabe K, Katayama K, Amano T. J Appl Polym Sci 1972;16:1077–91.
[17] Nakamura K, Katayama K, Amano T. J Appl Polym Sci 1973;17:1031–41.
[18] Sherwood CH, Price FP, Stein RS. J Polym Sci Polym Symp 1978;63:77–94.
[19] Coppola S, Grizzuti N, Maffettone PL. Macromolecules 2001;34:5030–6.
[20] Zheng R, Kennedy PK. J Rheol 2004;48(4):823–42.
[21] Van Meerveld J, Peters GWM, Hütter M. Rheol Acta 2004;44:119–34.
[22] Somani RH, Yang L, Hsiao BS, Sun T, Pogodina NV, Lustiger A. Macromolecules 2005;38:1244–55.
[23] Elmoumni A, Gonzalez-Ruiz RA, Coughlin EB, Winter HH. Macromol Chem Phys 2005;206:125–34.
[24] Bustos F, Cassagnau P, Fulchiron R. J Polym Sci Polym Phys 2006;44(11):1597–607.
[25] Lum FG, Carlston EF, Butler JC. U.S. Patent 2 766 211; 1956.
[26] Carlston EF, Lum FG. Ind Eng Chem Res 1957;49(8):1239–40.
[27] Ota T, Yamashita M, Yoshizaki O, Nagai E. J Polym Sci Polym Phys 1966;4:959–74.
[28] Ohta T, Fujiwara Y, Toshimori Y, Monobe K. Polymer 1992;33(8):1620–2.
[29] Inoue K. J Polym Sci Polym Phys 1985;23:743–50.
[30] Naudy S, Fulchiron R. Polym Eng Sci 2007;47:365–73.
[31] Lauritzen JI, Hoffman JD. J Appl Phys 1973;44(10):4340–52.
[32] Hernandez Sanchez F, Molina Mateo J, Romero Colomer FJ, Salmeron Sanchez M, Gomez Ribelles JL, Mano JF. Biomacromolecules 2005;6:3283–90.
[33] Huang TC, Tohara H, Blanton TN, Wu Y. J Appl Crystallogr 1993;26(2):180–4.
[34] Hoffman JD, Davis GT, Lauritzen Jr JI. In: Hannay NB, editor. Treatise on solid state chemistry, vol. 3. New York: Plenum; 1976 [chapter 7].
[35] Angelloz C, Fulchiron R, Douillard A, Chabert B, Fillit R, Vautrin A, et al. Macromolecules 2000;33:4138–45.
[36] Janeschitz-Kriegl H, Ratajski E, Stadlbauer M. Rheol Acta 2003;42:355–64.
[37] Janeschitz-Kriegl H. Colloid Polym Sci 2003;281:1157–71.
[38] Gruner JW. Z Kristallogr 1934;88:412–9.
[39] Wiewiora A, Sanchez-Soto PJ, Aviles MA, Justo A, Perez-Maqueda LA, Perez-Rodriguez JL, et al. Appl Clay Sci 1997;12:233–45.
[40] Bunn CW, Garner EV. Proc R Soc London Ser A 1947;189:39–68.
[41] Kim KJ, White JL. J Polym Sci Polym Phys 1999;37:1787–802.
[42] Ferrage E, Martin F, Boudet A, Petit S, Fourty G, Jouffret F, et al. Mater Sci 2002;37(8):1561–73.
[43] Naiki M, Fukui Y, Matsumura T, Nomura T, Matsuda M. J Appl Polym Sci 2001;79:1693–703.
[44] Obata Y, Sumitomo T, Ijitsu T, Matsuda M, Nomura T. Polym Eng Sci 2001;41(3):408–16.
[45] Choi WJ, Kim SC. Polymer 2004;45:2393–401.
[46] Santa Cruz C, Stribeck N, Zachmann HG, Balta Calleja FJ. Macromolecules 1991;24:5980–90.